JOURNAL OF SPACECRAFT AND ROCKETS
Vol. 29, No. 5, September–October 1992

Viscous Shock Layer Analysis of the Martian Aerothermal Environment

R. N. Gupta*
NASA Langley Research Center, Hampton, Virginia 23665
K. P. Lee†
Vigyan, Inc., Hampton, Virginia 23666
and
J. N. Moss* and K. Sutton‡
NASA Langley Research Center, Hampton, Virginia 23665

Detailed surface heating and flowfield results have been obtained for the stagnation region of a planetary exploration vehicle entering the Martian atmosphere. A viscous shock layer analysis (which includes an absorbing boundary layer) is used to obtain solutions with and without coupled ablation injection. Recently developed curve fits for the transport and thermodynamic properties of Martian atmospheric and ablation species as well as for the absorption coefficient for CO(4+) are employed. Extensive results are provided at altitudes of 30, 36, and 50 km for bodies with nose radii of 1, 2.3, and 23 m at freestream velocities of 6, 8, 10, and 12 km/s. Sublimation temperature is employed with coupled ablation injection cases, whereas radiative equilibrium wall temperature is used without injection. Only for bodies with large nose radii (23 m or larger) and for velocities of approximately 6 km/s can a reusable heat shield (with the currently available materials) be used. For higher velocities or vehicles with smaller nose radii, an ablative thermal protection system will be required. A comparison with thermochemical nonequilibrium calculations suggests that much of the flow in the shock layer is in thermochemical equilibrium for the cases analyzed. This is one of the first studies for the Martian entry conditions of large size bodies with coupled radiation and ablation injection.

Nomenclature

a_∞^* = speed of sound in freestream
C_i = mass frraction of species i, ρ_i^*/ρ^*
$\tilde{C}_l$ = mass fraction of element l, $\sum_i \delta_{il}(M_l^*/M_i^*)C_i$
C_p = frozen specific heat of mixture, $\sum_i C_i C_{p,i}$
$C_{p,i}$ = specific heat of species i, $c_{p,i}^*/c_{p,\infty}^*$
$D_{i,j}^*$ = binary diffusion coefficients
F_i^{0*} = free energy of species i at 1 atm (standard state)
H^* = enthalpy of mixtures, $h^* + (u^{*2}/2)$
h = enthalpy of mixture, $\sum_i C_i h_i$
h_a = enthaply of undecomposed ablation material
h_i = enthalpy of species i, h_i^*/U_∞^{*2}
K = thermal conductivity of mixture, $K^*/\mu^*(T_{\text{ref}}^*)C_{p,\infty}^*$
Le = Lewis number, $\rho^* D_{ij}^*(C_p^*/K^*)$
M_i^* = molecular weight of species i
$\dot{m}$ = mass injection rate, $\dot{m}^*/\rho_\infty^* U_\infty^*$
n = coordinate measured normal to body, n^*/R_N^*
Pr = Prandtl number, $\mu^* C_p^*/K^*$
p = pressure, $p^*/\rho_\infty^* U_\infty^{*2}$
Q = divergence of the net radiative heat flux, $Q^*/R_N^*/\rho_\infty^* U_\infty^{*3}$
$-q_{c,w}$ = convective heat flux toward the wall, $-(q_{\text{cond}} + q_{\text{diff}} + q_{\text{conv}})_w$, Eq. (5)
q_{cond} = heat flux due to conduction
q_{diff} = heat flux due to diffusion
q_r = net radiative heat flux in n direction, $q_r^*/\rho_\infty^* U_\infty^{*3}$
$q_r^{(+)*}$ = component of radiative flux toward the shock
$q_r^{(-)*}$ = component of radiative flux toward the wall
R_N^* = nose radius
R_{UNIV}^* = universal gas constant
s = coordinate measured along the body surface
T = temperature, T^*/T_{ref}^*
T_{REWT}^* = radiative equilibrium wall temperature
T_{ref}^* = reference temperature, $U_\infty^{*2}/C_{p,\infty}^*$
T_{sub}^* = sublimation temperature
U_∞^* = freestream velocity
u^* = velocity component tangent to body surface
ΔH_a^* = heat of ablation
$(\Delta h_i^f)_{T_{\text{ref}}}^*$ = standard heat of formation of species i at temperature T_{ref}
δ_{il} = number of atoms of the lth element in species i
δ_{sh}^* = shock standoff distance
$\bar{\epsilon}$ = Reynolds number parameter, $(u_{\text{ref}}^*/\rho_\infty^* R_N^* U_\infty^*)^{1/2}$
$\bar{\epsilon}$ = char emissivity, Eq. (7)
μ = viscosity of mixture, μ^*/μ_{ref}^*
ρ = density of mixture, ρ^*/ρ_∞^*
σ^* = Stefan-Boltzmann constant

Subscripts
A = ablator
i = ith species
j = jth species
l = lth element
sh = shock value
w = wall value
ν = radiation frequency
– = values for the solid ablation material at the surface

Superscripts
* = dimensional quantity

Received May 25, 1991; presented as Paper 91-1345 at the AIAA 26th Thermophysics Conference, Honolulu, HI, June 24–26, 1991; revision received Jan. 23, 1992; accepted for publication March 2, 1992.

*Aerospace Technologist, Aerothermodynamics Branch, Space Systems Division. Associate Fellow AIAA.
†Research Engineer. Member AIAA.
‡Head, Aerothermodynamics Branch, Space Systems Division. Associate Fellow AIAA.

Introduction

TO minimize the weight of space exploration vehicles, aerobraking is an effective alternative to an all-propulsive system for atmospheric insertion at both Mars and on return to Earth. Problems encountered during the high-energy entry into the Earth's atmosphere are analyzed in Ref. 1. This paper provides a similar treatment for high-energy entry and aerobraking into the Martian atmosphere.

In relation to the Earth-aerobraking velocities (12–15 km/s), the proposed velocities (6–10 km/s) for Mars aerobraking are much lower.[2,3] Therefore, unlike the Earth entry, radiative heating may not be significant for some of the Mars missions. However, with the increase in vehicle size and/or velocity, radiation could become dominant for evaluating the aerothermodynamic environment during the Mars entry. Further, for some of the aerobraking missions, total heating rates could become large enough to require an ablative thermal protection system.

Recently, Candler[4] and Park et al.[5] have evaluated the thermochemical nonequilibrium nature of the flow encountered by a vehicle entering the Martian atmosphere. Employing Camac's experimental values for the relaxation time,[6] Candler concluded that there is almost no thermal nonequilibrium due to the very fast vibrational relaxation of CO_2. His calculations, based on the full Navier-Stokes equations with a nonionized eight-species chemical kinetics model, show the presence of a relatively thin shock with a viscous layer dominant near the surface for the cases analyzed. Grid resolution, of course, plays an important role in establishing the shock thickness and, consequently, affects the relaxation rates in the shock layer. Candler, however, did not include a collision-limiting term[5] in Camac's expression for relaxation time. Since Camac's data are for a maximum temperature of about 6000 K, inclusion of a collision-limiting term (which dominates at high temperatures) would slow down the vibrational relaxation of CO_2 to some extent at high temperatures immediately behind the shock. A value of 10^{-18} cm^2 for the collision-limiting cross section of CO_2 used by Park et al., however, is too small and does not give[7] the proper relaxation rate at temperatures of about 6000 K and less when compared with Camac's data. Based on Candler's calculations,[7] it appears that a limiting cross section of the order of 10^{-16} cm^2 may be more appropriate for CO_2 relaxation. These calculations further imply a much smaller thermal nonequilibrium region (closer to Candler's earlier calculations[4]) than the predictions of Park et al.[5] This suggests that the use of a single temperature gas model would be a reasonable approximation. Furthermore, computationally more efficient solution methods [such as the viscous shock layer (VSL) method] could be used for such flows, especially if radiatively coupled solutions are to be obtained. Candler's calculations did not contain any coupling to the radiative cooling of the shock layer gases.

Also, Rochelle et al.[8] recently analyzed the aerothermodynamic environment for Mars entry and Mars return aerobraking missions. They provided uncoupled results (using two different flowfield descriptions) for the convective and radiative heating for a 97% CO_2 and 3% N_2 Martian atmosphere, assuming the flowfield to be in chemical equilibrium. Their convective heating results were obtained from a boundary-layer analysis, whereas the radiative heat transfer results were obtained from an inviscid nongray radiation-coupled method of Ref. 9.

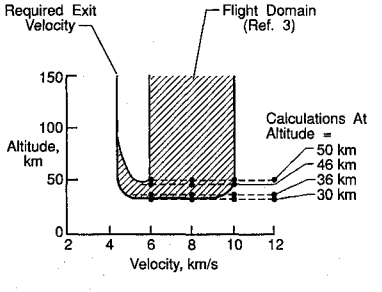

Fig. 1 Flight domain for Mars aerobraking studies.

Moss et al.[10] carried out a viscous shock layer analysis earlier for the Pioneer Venus probe. Their results suggested that the radiative heating rates obtained with inviscid analyses are significantly (as much as 30%) greater than those obtained with a nonablating viscous shock layer analysis. The agreement between inviscid and VSL radiative heating results is acceptable only when the effect of a strongly absorbing boundary layer (which is included in the VSL analysis) is accounted for in the inviscid calculations.

Tauber et al.[11–13] have conducted Mars mission studies in the recent past. However, the heating environments from these studies were not coupled. References 14 and 15, however, have presented some coupled radiation/ablation solutions using an inverse procedure, which assumes a shock shape, then proceeds downstream, predicting a body shape. In comparison, the method of Refs. 1, 10, and 16 employs a direct procedure, which solves the governing equations for a given body shape.

In this study, we present results from a viscous shock layer analysis for the high-energy flowfield under chemical equilibrium for Mars entry conditions. This analysis is based on the work of Refs. 1, 10, and 16. The focus of the present calculations is on evaluating the flowfield around bodies for Mars entry conditions in the velocity range of 6–12 km/s and altitudes of 30–50 km (see Fig. 1).

Results presented here are based on the transport and thermodynamic properties for the C-H-N-O system given in Ref. 1. Calculations are carried out by employing the radiative equilibrium wall temperature for no ablation injection cases. For the coupled carbon-phenolic calculations, sublimation temperatures for the carbon-phenolic ablator have been employed. Results provided include an estimate of the chemical nonequilibrium in the flowfield for the case of no injection and radiation.

Analysis

Flowfield Model and Method of Solution

The flow in the shock layer is assumed to be axisymmetric, steady, laminar, viscous, and compressible over a body similar to that used for the Earth entry study in Ref. 1. The viscous shock layer equations employed to analyze such a flow are those of a multicomponent radiating gas mixture under chemical equilibrium conditions.[16] The present analysis provides for ablation injection at the surface and includes a detailed description of the radiative transport,[17] equilibrium chemistry, and thermodynamic and transport properties. The governing equations are solved as a parabolic set of equations using an implicit, finite difference, numerical procedure. The VSL analysis, therefore, provides a direct means of accounting for interactions between the inviscid and viscous flow regions due to radiative transfer, inviscid entropy layer swallowing, and mass injection. The present method of solution is similar to that of Ref. 16 and therefore is not presented here.

Boundary Conditions

The boundary conditions employed at the shock are those obtained by using the Rankine-Hugoniot relations. No-slip continuum boundary conditions are used at the body surface. The wall temperature is either specified or calculated. For the calculated conditions, where the surface heating is insufficient to produce sublimation, the surface temperature is assumed to be the radiative equilibrium wall value obtained from

$$T^*_{\mathrm{REWT}} = \left\{ \left[q_r^{(-)} - \bar{\epsilon}^2 \left(K \frac{\partial T}{\partial n} + \frac{\mu Le}{Pr} \sum_{i=1}^{NS} h_i \frac{\partial C_i}{\partial n} \right) \right] \frac{\rho^*_\infty U^{*3}_\infty}{\bar{\epsilon}\sigma^*} \right\}^{1/4} \quad (1)$$

For the cases with surface ablation, a wall sublimation temperature is used. For such solutions, the coupled mass injection

rate for steady-state ablation is obtained from

$$\dot{m} = \left[\frac{-q^*_{c,w} - q^*_{r,w}}{\sum_{i=1}^{NS}(C_i h^*_i)_w - h^*_a}\right] \Big/ (\rho^*_\infty U^*_\infty) \tag{2a}$$

or

$$\dot{m} = \left[\frac{-q^*_{c,w} - q^*_{r,w}}{\Delta H^*_a}\right] \Big/ (\rho^*_\infty U^*_\infty) \tag{2b}$$

and the sublimation temperature and heat of ablation for a carbon-phenolic ablator are computed from:

$$T^*_{sub} = 3736.0 + 306.0 \log p^* + 26.0 (\log p^*)^2, \text{ K} \tag{3a}$$

$$\Delta H^*_a = 5951.3 - 430.2 \log p^* + 262.9 (\log p^*)^2, \text{ kcal/kg} \tag{3b}$$

where p^* is the wall pressure in atmospheres. These equations are applicable for surface pressures of 0.01-10.0 atm and for the condition where the gas species adjacent to the surface are solely due to the ablation species. The surface temperature and the coupled mass injection rate are calculated by iterating the solution of the governing flowfield equations and the surface boundary conditions given by Eqs. (2) and (3).

For ablation injection, the elemental concentrations at the wall are governed by convection and diffusion and are obtained from the equations

$$\left(\frac{\partial \tilde{C}_l}{\partial n}\right)_w - \frac{1}{\tilde{\epsilon}^2}\left(\frac{Pr}{\mu Le}\right)_w [(\tilde{C}_l)_w - (\tilde{C}_l)_-] = 0 \tag{4}$$

and the heat transferred to the wall because of conduction, diffusion, and convection is

$$-q_{c,w} = \tilde{\epsilon}^2\left[K\frac{\partial T}{\partial n} + \frac{\mu Le}{Pr}\sum_{i=1}^{NS} h_i \frac{\partial C_i}{\partial n} - \dot{m}\sum_{i=1}^{NS}(C_i h_i - C_{i-} h_{i-})\right]_w \tag{5}$$

For the radiative transport calculations, the bow shock is considered transparent and the freestream is considered cold and transparent. Therefore, the precusor effects are neglected. Further, the body surface is assumed to be gray with a reflectivity of 0.15, emissivity of 0.85, and transmissivity of 0. The energy reradiated from the surface is included both in the radiation transport calculation as well in the surface energy balance [Eq. (2)] . The net radiative flux can be represented as

$$q_r = q_r^{(+)} - q_r^{(-)} \tag{6}$$

At the surface

$$q^{(+)*}_{r,w} = \tilde{\epsilon}\sigma^* T^{*4}_w \tag{7}$$

Radiative Transport

The radiation transport code RADICAL[17,18] has been used to compute radiative flux q_r and the divergence of radiative flux Q. This code accounts for the effects of nongray self-absorption and includes the molecular band, continuum, and atomic line transitions. Fourteen chemical species are considered for computing the radiative transport in the Martian atmosphere: O, O_2, O^+, N, N_2, e^-, C, C_2, C_3, CO, CO_2, CN, C^+, and CO^+. Inclusion of five more species (O_2^+, N^+, N_2^+, NO, and NO^+) did not affect the radiative transport to any appreciable degree in absence of ablation. For ablation injection, 20 chemical species are used: the 14 used for no injection plus H, H_2, HCN, C_2H, C_3H, and C_4H. The ultraviolet radiation properties used here for C_3 are those of Ref. 19. The thermodynamic properties employed for the various species are those of Refs. 1 and 20 and those given in the next section.

Thermodynamic and Transport Properties

A free-energy minimization calculation procedure[21] is used to obtain the equilibrium composition. Thermodynamic properties of specific heat, enthalpy, and free-energy and transport properties for viscosity and thermal conductivity are required for each species considered. Values of the thermodynamic and transport properties for C-H-N-O species (required for the Martian atmosphere shock layer species and ablation products) are obtained from the polynominal curve fits of Refs. 1, 20, and 22. [Constant $A_{\mu_{CO_2}}$ (for viscosity curve fits) given in Table III of Ref. 22 should be 0.0204.] Mixture viscosity is obtained by using the semiempirical formula of Wilke.[23] A similar relation[23] is used to compute the mixture thermal conductivity. A variable Prandtl number along with either a constant or a variable Lewis number is used. A value of 1.4 is used for the constant Lewis number calculation, and a binary diffusion approximation is used for computing the variable Lewis number. The binary diffusion coefficient at low velocities is assumed to be that for CO diffusing into atomic oxygen, whereas at high velocities it is taken to be that for C (gas) diffusing into atomic oxygen. For a relatively cool surface (with temperatures around 1000 K), the surface heat transfer is calculated with a binary diffusion coefficient based on CO_2 and N_2. For higher wall temperatures, it is computed with the assumption of CO diffusing into atomic oxygen.

Results and Discussion

Results are presented for coupled mass injection rates with equilibrium flowfield chemistry for the high-energy entry into the Martian atmosphere. The injectants considered are carbon-phenolic ablation species. The calculated results are for the freestream conditions summarized in Table 1. The atmospheric composition used in the present calculations is 97% CO_2 and 3% N_2, by mass. The freestream conditions of Table 1 are from the atmospheric model of the Committee on Space Research north summer mean (COSPAR NS mean) as tabulated by Pitts et al.[24] For brevity, only a graphical display of results is provided here. Detailed tabulated results, however, are given in Ref. 22.

Effect of Boundary-Layer Absorption

Figure 2 demonstrates the influence of an absorbing boundary larger on the radiative heat transfer to the surface. This figure compares the VSL surface radiative heating rates with those obtained from the inviscid flowfield analysis[25] for a body with a nose radius of 6.6 m. The heating rates obtained with the VSL method are, in general, less than those obtained with the inviscid analysis. The maximum difference between the VSL and inviscid results is near the surface and is primarily due to the inclusion of a strongly absorbing boundary layer in

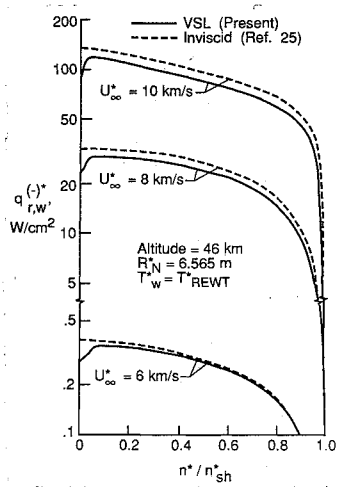

Fig. 2 Boundary-layer absorption of stagnation incident radiative flux profiles for Martian atmosphere; $(C_{CO_2})_\infty = 0.97$, $(C_{N_2}) = 0.03$.

Table 1 Freestream conditions for the Martian atmosphere ($C_{CO_2} = 0.97$ and $C_{N_2} = 0.03$)

Altitude, km	ρ_∞^*, kg/m^3	T_∞^*, K	P_∞^*, N/m^2	a_∞^*, km/s	u_∞^*, km/s	Effective nose radius R_N^*, m
30	9.80×10^{-4}	175.0	32.8	0.213	6, 8, 10, 12	1.0, 2.3, 23.0
36	5.24×10^{-4}	167.5	16.8	0.209	6, 8, 10, 12	1.0, 2.3, 23.0
46	1.73×10^{-4}	156.0	5.15	0.202	6, 8, 10	6.57
50	1.08×10^{-4}	152.2	3.15	0.200	6, 8, 10, 12	1.0, 2.3, 23.0

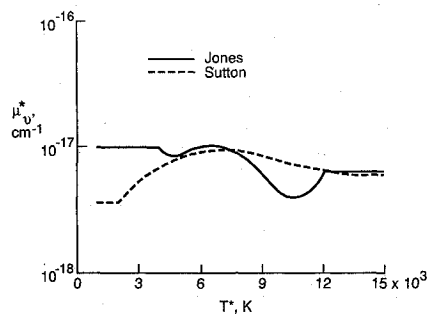

Fig. 3 Absorption coefficient for CO(4+) from the two curve fits at the band head ($h_\nu = 8.0$ eV).

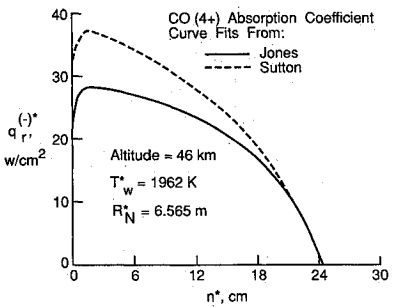

Fig. 4 Effect of CO(4+) absorption coefficient on stagnation-point radiative heat flux ($U_\infty^* = 8$ km/s, $\dot{m} = 0$).

the VSL solution. The inviscid heating value is about 50% greater than the corresponding VSL value at the surface at a velocity of 10 km/s. This difference is about 40% at 6 km/s velocity.

Effect of Flowfield Properties on Surface Heating

In this study, an evaluation is made of the flowfield properties affecting the radiative and convective heating. The absorption coefficient of CO(4+) affects the radiative heating significantly, whereas the effect of using a constant or variable Lewis number (with a variable *Pr*) on convective heating without ablation is negligible.

Effect of CO(4+) Absorption Coefficient

Figure 3 shows the absorption coefficient values for CO(4+) obtained from the curve fits (one of the present authors) at a photon energy of 8.0 eV, where the band head lies. Jones curve-fitted the values of Ref. 26 in the temperature range 4000–12,000 K. Using similar reference values as those of Ref. 26, Sutton computed and curve-fitted the CO(4+) absorption coefficient values from 2000–14,000 K. Outside of the temperature range for which the data were curve-fitted, the implementation of these data assumed a constant value for the absorption coefficient at either the lower or upper temperature limits as shown in Fig. 3. The radiative heating predictions of Refs. 10 and 25 are based on the curve fits of Jones.

Figure 4 shows the effect of using the two curve fits for absorption coefficient on the incident radiation. The differences in the two curve fits have an impact on the radiative heat flux through the entire shock layer. Radiative heat transfer values computed by using Jones' curve-fit values for the CO(4+) absorption coefficient are smaller than those obtained using Sutton's curve-fit values. The radiative equilibrium wall temperature and the convective heating rates are affected to a much lesser extent.

Calculations for Mars Entry

Chemical Equilibrium

After evaluating the effects of boundary-layer absorption and CO(4+) absorption coefficient (the two most important factors affecting the radiative heating), results are now presented for the four velocities (i.e., 6, 8, 10, and 12 km/s) at

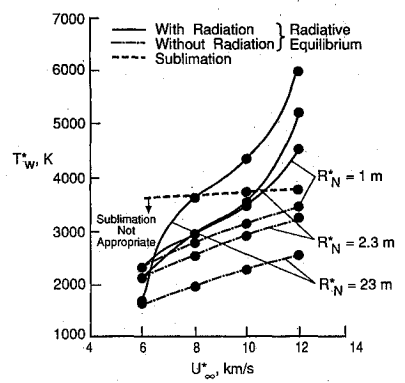

a) Alt = 30 km

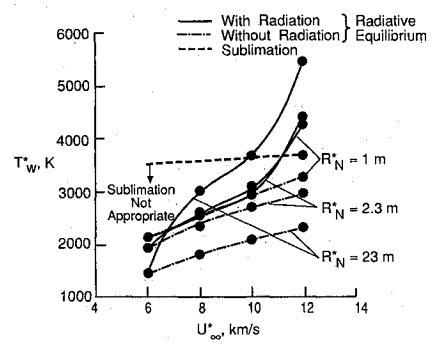

b) Alt = 36 km

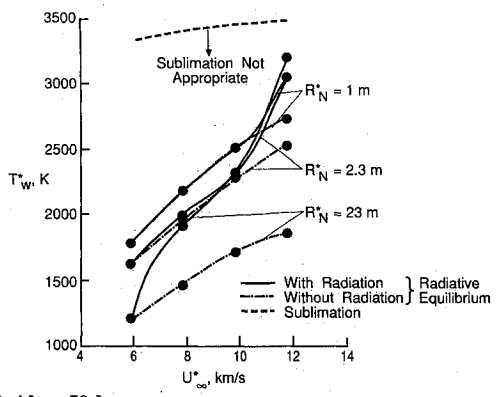

c) Alt = 50 km

Fig. 5 Stagnation-point sublimation and radiative equilibrium wall temperatures with and without coupled ablation injection, respectively.

three altitudes (i.e., 30, 36, and 50 km) shown in Fig. 1. Bodies with nose radii of 1, 2.3, and 23 m are considered. The freestream conditions are provided in Table 1. The radiation absorption coefficient for CO(4+) is obtained from the curve fits of Sutton.

The sublimation as well as the radiative equilibrium wall temperatures are shown in Fig. 5 for the various trajectory points for different body sizes analyzed here. For the freestream velocities considered, only that at 12 km/s is sufficient to cause sublimation for the three nose-radii bodies considered at altitudes of 30 and 36 km. At an altitude of 50 km (Fig. 5c), the surface heating is insufficient to cause sublimation for the velocities and body sizes considered. Figure 5 provides the maximum values for the wall temperature one may expect for the cases considered. As shown, for example, in Fig. 5a, the maximum temperatures would lie below the sublimation curve for bodies of all nose radii at velocities less than or equal to 8 km/s. For velocities greater than about 10.6 km/s, the maximum possible temperature for all nose radii are those corresponding to the respective sublimation value.

It may be seen from Fig. 6 that the 23 m nose radius gives the minimum surface temperature for velocities near 6 km/s, whereas the 2.3 m nose radius yields the minimum temperature near 8 km/s. A vehicle with a nose radius smaller than 23 m would produce a reduction in surface temperature for the higher velocity conditions; 1 m nose radius gives the minimum temperature. For the cases where sublimation is appropriate, surface temperature corrsponds to the sublimation temperature of the ablator and is independent of the nose radius. Figure 6 also shows the temperature limit of 1850 K for the reusable heat shield. This temperature correponds to a heat flux of 50 W/cm^2 under the assumption of radiative equilibrium. For currently available material for the reusable heat shield, 50 W/cm^2 is the maximum allowable value of the heat flux reaching the surface. As can be noticed from Fig. 6, only vehicles with a nose radius of about 23 m can employ a reusable heat shield at a velocity of about 6 km/s.

Figure 7 shows the stagnation-point convective heat flux for different nose radii bodies corresponding to the surface temperature of Fig. 5. For the coupled ablation injection cases, reduction in convective heating is considerable as seen from Fig. 7.

The incident radiative heat flux is shown in Fig. 8. There is considerable reduction in the radiative heat flux due to coupled ablation injection, even though the percent reduction in value is not as large as in the case of convective heat flux. Since radiative flux is generally dominant and has a large value for large size bodies (especially at higher velocities), the reduction due to ablation injection is quite significant. Further, a comparison of values from Figs. 7 and 8 shows that radiative and convective heat fluxes are comparable for all three nose radii bodies considered at velocities between 8 and 10 km/s, except for the large nose radius body ($R_N^* = 23$ m) at low altitudes and the small nose radius body ($R_N^* = 1$ m) at high altitudes.

The stagnation-point total heating rate results shown in Fig. 9 indicate that a vehicle with a nose radius smaller than 23 m would produce a reduction in combined convective and radiative heating for the higher velocity conditions. For velocities near 6 km/s, the 23 m nose radius is close to an optimal size for achieving a minimum heating rate, whereas near 8 km/s, the 2.3 m nose radius yields the minimum heating. For 10 km/s and greater velocities, the 1 m nose radius would produce minimum heating rates. As mentioned earlier, currently available material for the reusable heat shield cannot withstand heating rates above 50 W/cm^2; only the 23 m nose radius vehicle can be used with such a heat-shield at a velocity of about 6 km/s. (A velocity of 6 km/s is the velocity obtained from a minimum energy interplanetary transfer[3] and is needed to affect a rendezvous with planet Mars.) For higher velocities or smaller nose radii vehicles, an ablative thermal protection system will be required. [For flow conditions, where the surface heating is insufficient to cause sublimation and yet large enough so that the reusable heat shields cannot be used, use of an ablative thermal protection system would still be needed.

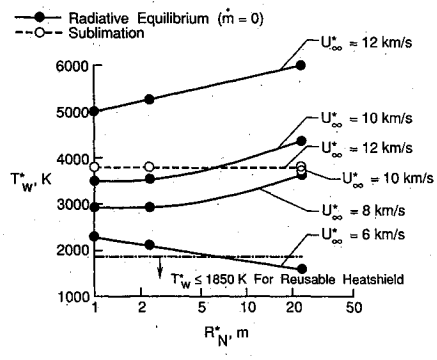

Fig. 6 Stagnation-point temperature for 30 km altitude.

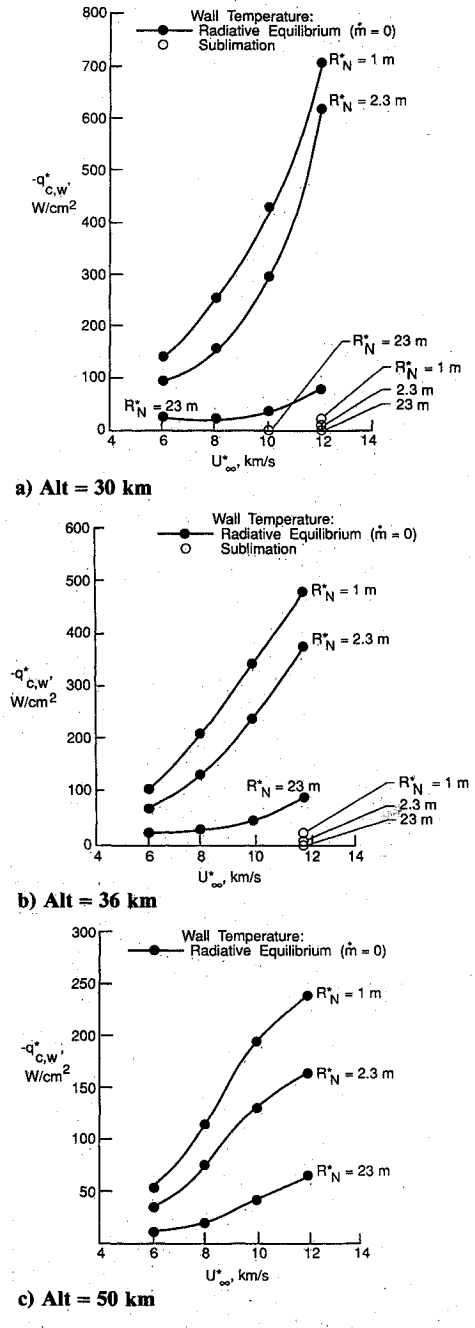

Fig. 7 Stagnation-point convective heat flux for different Martian entry velocities with and without ablation injection.

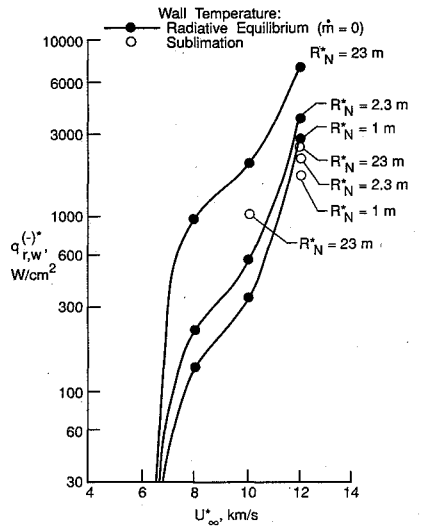

a) Alt = 30 km

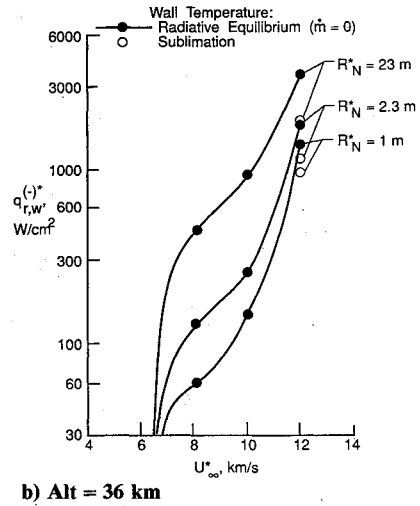

b) Alt = 36 km

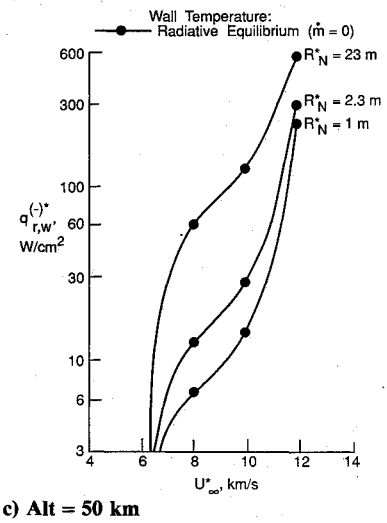

c) Alt = 50 km

Fig. 8 Stagnation-point radiative heat flux for different Martian entry velocities with and without coupled ablation injection.

For such cases, ablation products (obtained from pyrolysis and char removal due to oxidation) would still be injected into the flowfield and would result in surface temperatures lower than the corresponding radiative equilibrium wall temperatures obtained with no surface injection.]

Figures 10–12 show stagnation profiles for various flowfield quantities with coupled ablation injection using a carbon-phenolic heatshield. These profiles are for a 2.3 m nose radius body at an altitude of 30 km and a freestream velocity of 12 km/s. Figure 10 gives profiles for the nondimensional values of tangential velocity (u^*/u^*_{sh}), temperature (T^*/T^*_{sh}), mass flux normal to the surface $[\rho^* v^*/(\rho^* v^*)_{sh}]$, enthalpy ($H^*/H^*_{sh}$) net radiative heat flux q^*_r, divergence of the net radiative heat

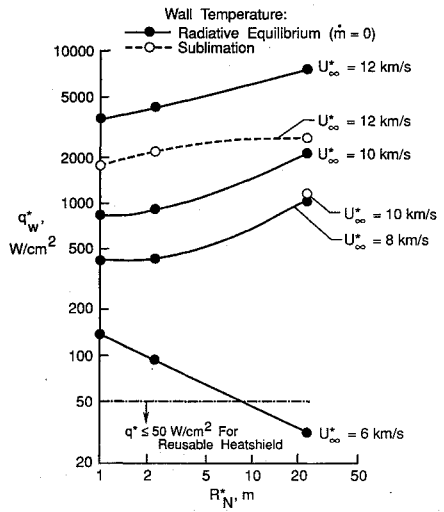

Fig. 9 Stagnation-point total heat flux for 30 km altitude.

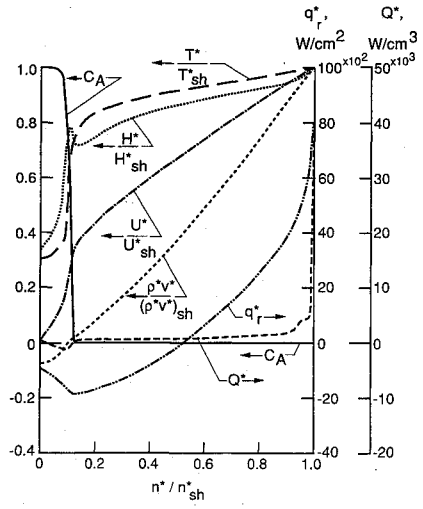

Fig. 10 Stagnation profiles for various flowfield quantities with coupled ablation injection ($\dot{m}$ = 0.075) with carbon phenolic (Alt = 30 km, R^*_N = 2.3 m, U^*_∞ = 12 km/s).

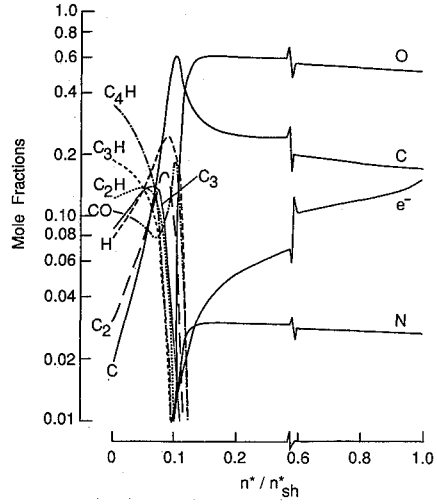

Fig. 11 Mole fraction profiles for major species with coupled ablation injection ($\dot{m}$ = 0.075) with carbon phenolic (Alt = 30 km, R^*_N = 2.3 m, U^*_∞ = 12 km/s).

flux Q^*, and ablator mass fraction C_A. The normal mass flux at the surface is the coupled ablation injection value of 0.075. Positive values of the radiative flux q_r^* indicate net radiative heat flux away from the surface, whereas negative values indicate net flux toward the surface. There is a bulge (similar to the ones noted in earlier studies of Refs. 1 and 27) in the enthalpy profile at a distance (n^*/n_{sh}^*) of about 0.1 from the surface. The bulge appears to occur where the flowfield composition undergoes a transition from freestream to ablation species, as evidenced by the ablator mass fraction C_A profile. Further, the location of enthalpy bulge coincided with the location of maximum radiative absorption (indicated by negative values of the divergence of heat flux Q^*).

The mole fraction of the major flowfield species is shown in Fig. 11. The transition from the Martian atmospheric species to ablation species as well as the maximum concentration of neutral carbon species occurs in a location where the enthalpy bulge appears. The neutral carbon species are quite effective in blocking the radiative flux component $q_r^{(-)*}$ directed toward the surface as shown in Fig. 12. Clearly, the values are reduced where the enthalpy bulge appears, i.e., in the vicinity of $n^*/n_{sh}^* = 0.1$.

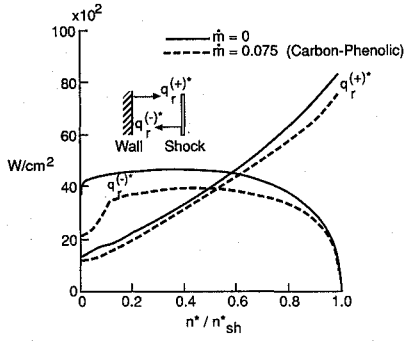

Fig. 12 Effect of ablation injection (coupled) on radiative heat flux components [Alt = 30 km, $R_N^* = 2.3$ m, $U_\infty^* = 12$ km/s, $T_W^* = 3772(T_{sub}^*)$].

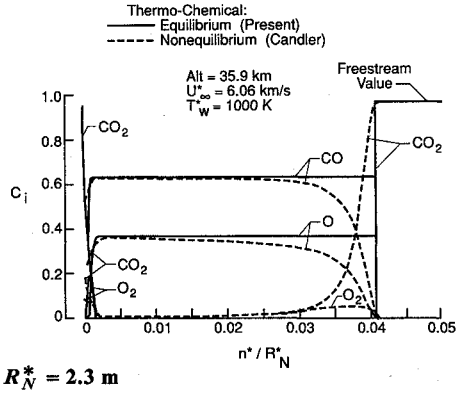

a) $R_N^* = 2.3$ m

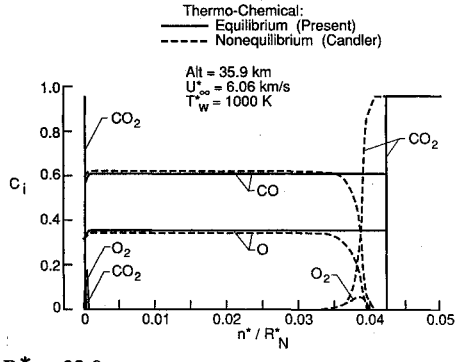

b) $R_N^* = 23.0$ m

Fig. 13 Comparison of stagnation streamline concentration profiles for Martian atmosphere; $(C_{CO_2}) = 0.9685$, $(C_{N_2})_\infty = 0.0315$.

Comparisons with Thermochemical Nonequilibrium Results

Based on Camac's[6] experimental values for the vibration relaxation of CO_2, Candler[4] concluded that there is very little thermal nonequilibrium in the flowfield. Figure 13 shows the extent of chemical nonequilibrium. Clearly, much of the shock layer for both small (Fig. 13a) and large (Fig. 13b) nose radius bodies is in chemical equilibrium. There appears to be a narrow region close to the surface where some chemical nonequilibrium persists. Results of Ref. 4, however, are not yet conclusive as large nose radius results from this reference (shown in Fig. 13b) indicate no CO_2 at the surface, whereas there is a considerable amount of CO_2 shown for a smaller nose radius body from the same reference in Fig. 13a. Generally, flowfields around larger nose radii bodies would be closer to equilibrium conditions. It should be mentioned here that different boundary conditions are employed in Candler's and the present calculations. Candler's results are obtained with a fully noncatalytic wall boundary condition, which yields the lowest convective heating values possible. The present results are for an equilibrium wall. These differences in the boundary conditions are also responsible for the discrepancy between the two predictions near the surface shown in Fig. 13. The discrepancy may also be attributed to the existence of nonequilibrium in the boundary layer. However, from the comparisons presented here, it appears that for bodies with $R_N > 2.3$ m and altitudes less than about 36 km, much of the flowfield in the shock layer is in thermochemical equilibrium—an assumption made in obtaining the present results.

Conclusions

Surface heating and flowfield results are presented for the stagnation region of a planetary exploration vehicle entering the Martian atmosphere. Solutions for the high-energy viscous flowfields with complete radiative heating are obtained from a viscous shock layer analysis for laminar flow under chemical equilibrium conditions. Results are presented with and without coupled radiation ablation injection using the recently developed curve fits for the transport and thermodynamic properties of Martian atmospheric and ablation species. The present analysis includes a strongly absorbing boundary layer and, consequently, gives considerably lower radiative heat transfer rates than those obtained from inviscid analyses. The radiative heating results have been obtained with the new curve fits for CO(4+) absorption coefficient and are significantly greater than those computed using the previous curve fits to Woodward's data.

Detailed results are provided at altitudes of 30, 36, and 50 km for bodies with effective nose radii of 1, 2.3, and 23 m at freestream velocities of 6, 8, 10, and 12 km/s. These results are for the heating conditions that may be encountered by the proposed exploration vehicles to planet Mars. Sublimation temperature is employed with coupled radiation injection cases, whereas radiative equilibrium wall temperature is used without injection. Even for cases where the surface heating is insufficient to cause sublimation, a reusable heat shield with the currently available materials cannot be used. Only for bodies with large nose radii (23 m or larger) and for velocities of about 6 km/s or less can such a heat shield be considered. For higher velocities or smaller nose radii vehicles, an ablative thermal protection system will be required. A comparison with thermochemical nonequilibrium calculations suggests that, except for bodies with nose radii less than about 2.3 m and altitudes greater than 36 km, much of the flow in the shock layer appears to be in thermochemical equilibrium. This is one of the first studies for the Martian entry conditions of large size bodies with coupled radiation and ablation injection.

Acknowledgment

We are grateful to Lin Hartung for providing most of the calculations reported here from the inviscid flowfield analysis with coupled radiation.

References

[1]Gupta, R. N., Lee, K. P., Moss, J. N., and Sutton, K., "Viscous Shock Layer Solutions with Coupled Radiation and Ablation Injection for Earth Entry," AIAA Paper 90-1697, June 1990.

[2]Walberg, G. D., "A Review of Aerobraking for Mars Missions," International Astronautical Federation, Paper 88-196, Oct. 1988.

[3]Braun, R. D., Powell, R. W., and Hartung, L. C., "Effect of Interplanetary Trajectory Options on a Manned Mars Aerobrake Configuration," NASA TP-3019, Aug. 1990.

[4]Candler, G. V., "Computation of Thermochemical Nonequilibrium Martian Entry Flow," AIAA Paper 90-1695, June 1990.

[5]Park, C., Howe, J. T., Jaffe, R. L., and Candler, G. V., "Chemical-Kinetic Problems of Future NASA Missions," AIAA Paper 91-0464, Jan. 1991.

[6]Camac, M., "CO_2 Relaxation Processes in Shock Waves," *Fundamental Phenomena in Hypersonic Flow,* edited by J. G. Hall, Cornell Univ. Press, Ithaca, NY, 1966, pp. 195–215.

[7]Candler, G. V., private communication, North Carolina State Univ., Raleigh, NC, Feb. 1991.

[8]Rochelle, W. C., Bouslog, S. A., Ting, P. C., and Curry, D. M., "Aerothermodynamic Environment for Mars Entry, Mars Return, and Lunar Return Aerobraking Missions," AIAA Paper 90-1701, June 1990.

[9]Hartung, L. C., Sutton, K., and Brauns, F., "Equilibrium Radiative Heating Tables for Aerobraking in the Martian Atmosphere," NASA TM-1022659, May 1990.

[10]Moss, J. N., Zoby, E. V., Sutton, K., and Anderson, E. C., "Aerothermal Environment for the Pioneer Venus Multiprobe Mission," *Aerodynamic Heating and Thermal Protection Systems,* edited by Leroy S. Fletcher, Vol. 59, Progress in Astronautics and Aeronautics, AIAA, New York, 1977, pp. 3–26.

[11]Tauber, M., Bowles, J., and Yang, L., "The Use of Atmospheric Braking During Mars Missions," AIAA Paper 89-1730, June 1989.

[12]Tauber, M., Palmer, G., and Yang, L., "Earth Atmospheric Entry Studies for Manned Mars Missions," AIAA Paper 90-1699, June 1990.

[13]Tauber, M., Chargin, M., Henline, W., Chiu, A., Yang, L., Hamm, K. R., Jr., and Miura, H., "Aerobrake Design Studies for Manned Mars Missions," AIAA Paper 91-1344, June 1991.

[14]Park, C. and Milos, F. S., "Computational Equations for Radiating and Ablating Shock Layers," AIAA Paper 90-0356, Jan. 1990.

[15]Henline, W. D., "Aerothermodynamic Heating Environment and Thermal Protection Materials Comparison for Manned Mars-Earth Return Vehicles," AIAA Paper 91-0697, Jan. 1991.

[16]Moss, J. N., "Reacting Viscous Shock Layer Solution with Multicomponent Diffusion and Mass Injection," NASA TR R-411, June 1974.

[17]Nicolet, W. E., "Advanced Methods for Calculating Radiation Transport in Ablation Product Contaminated Boundary Layers," NASA CR-1656, Sept. 1970.

[18]Nicolet, W. E., "User's Manual for the Generalized Radiation Transfer Code (RAD/EQUIL)," NASA CR-116353, Oct. 1969.

[19]Shinn, J. L., "Optical Absorption of Carbon and Hydrocarbon Species from Shock Heated Acetylene and Methane in the 135-220 m Wavelength Range," *Thermophysics of Atmospheric Entry,* edited by T.E. Horton, Vol. 82, Progress in Astronautics and Aeronautics, AIAA, New York, 1982, pp. 68–80.

[20]Gupta, R. N., Yos, J. M., Thompson, R. A., and Lee, K. P., "A Review of Reaction Rates and Thermodynamic and Transport Properties for an Eleven-Species Air Model for Chemical and Thermal Nonequilibrium Calculations to 30000 K," NASA RP-1232, Aug. 1990.

[21]Stroud, C. W., and Brinkley, K. L., "Chemical Equilibrium of Ablation Materials Including Condensed Species," NASA TN D-5391, Aug. 1969.

[22]Gupta, R. N., Lee, K. P., Moss, J. N., and Sutton, K., "A Viscous-Shock-Layer Analysis of the Martian Aerothermal Environment," AIAA Paper 91-1345, June 1991.

[23]Bird, R. B., Stewart, W. E., and Lightfoot, E. N., *Transport Phenomena,* Wiley, New York, 1960, pp. 24 and 258.

[24]Pitts, D. E., Tillman, J. E., Pollack, J., and Zurek, R., "Model Profiles of the Mars Atmosphere for the Mars Rover and Sample Return Mission," Unpublished Rept., NASA Johnson Space Center, Houston, TX, 1990.

[25]Sutton, K., "Fully Coupled Nongray Radiating Gas Flows with Ablation Product Effects About Planetary Entry Bodies," *AIAA Journal,* Vol. 12, No. 8, 1974, pp. 1033–1105.

[26]Woodward, H. T., "Predictions of Shock-Layer Radiation from Molecular Band Systems in Proposed Planetary Atmospheres," NASA TN D-3850, Oct. 1966.

[27]Moss, J. N., "Radiative Viscous-Shock-Layer Solutions with Coupled Ablation Injection," *AIAA Journal,* Vol. 14, No. 9, 1976, pp. 1311-1317.

Gerald T. Chrusciel
Associate Editor